Available online at www.jrors.ir

JRORS Journal Of Radar and Optic Remote Sensing

**Journal Of Radar and Optic Remote Sensing**

JRORS 1 (2018) 36–57

# Evaluation of super-resolution algorithm for detection and recognition of features from MODIS and OLI images at sub-pixel scale using Hopfield Neural Network

Mohammad Hosein Mehrzadeh Abarghooee [a*] , Ali Sarkargar Ardakani[b]

[a] *Ms in GIS&RS,Yazd Branch, Islamic Azad University, Yazd, Iran*
[b] *GIS&RS Department, Yazd Branch, Islamic Azad University, yazd, Iran*

Received 12 February 2018; revised 9 April 2018; accepted 10 June 2018

## Abstract

Fuzzy classification techniques have been developed recently to estimate the class composition of image pixels, but their output provides no indication of how these classes are distributed spatially within the instantaneous field of view represented by the pixel. Super-resolution land-cover mapping is a promising technology for prediction of the spatial distribution of each land-cover class at the sub-pixel scale. This distribution is often determined based on the principle of spatial dependence and from land-cover fraction images derived with soft classification technology. As such, while the accuracy of land cover target identification has been improved using fuzzy classification, it remains for robust techniques that provide better spatial representation of land cover to be developed. An approach was adopted that used the output from a fuzzy classification to constrain a Hopfield neural network formulated as an energy minimization tool. The network converges to a minimum of an energy function. This energy minimum represents a "best guess" map of the spatial distribution of class components in each pixel. The technique was applied to remote sensing imagery (MODIS & OLI images), and the resultant maps provided an accurate and improved representation of the land covers. Low RMSE, high accuracy. By using a Hopfield neural network, more accurate measures of land cover targets can be obtained, The

* Corresponding author. Tel: +98- 3537305726.
*E-mail address:* hosein_mehrzade@yahoo.com.

Hopfield neural network used in this way represents a simple, robust, and efficient technique, and results suggest that it is a useful tool for identifying land cover targets from remotely sensed imagery at the sub-pixel scale. The present research purpose was evaluation of HNN algorithm efficiency for different land covers (Land, Water, Agriculture land and Vegetation) through Area Error Proportion, RMSE and Correlation coefficient parameters on MODIS & OLI images and related ranking, results of present super resolution algorithm has shown that according to precedence, most improvement in feature's recognition happened for Water, Land, Agriculture land and ad last Vegetation with RMSEs 0.044, 0.072, 0.1 and 0.108.

*Keywords:* Fuzzy classification, Hopfield Neural Network, Spatial resolution, Sub-pixel, Land cover, Energy function, Super resolution

## 1. Introduction

Since land cover information is important in the field of management and understanding the environment, extraction and characterization of the location of different land covers as accurately as possible has been a necessary process for many applications such as military, spyware, agricultural planning, water management, etc., and remote sensing technology has made it possible by providing wide and consistent imaging of all points of the earth (for different sensors from 3 hours to 16 days different) (Tatem et al., 2001).

The development of remote sensing technology has enabled the storage of great amount of fine spatial resolution remotely sensed images. These data can provide fine-resolution land cover spatial information and are promising in reducing the SRM uncertainty (Xiaodong et al., 2014). The mixed pixel problem strongly affects the accuracy in extracting land cover information from remotely sensed images (Lu et al., 2011b).

The basic and predominant solution to the interpretation of mixed pixels is based on the fuzzy classification algorithm, but with none of the fuzzy classification methods, the location and position of the land cover class on sub-pixel scale are not determined and for this, it was necessary to use other methods such as super-mapping based on the Hopfield neural network (Tatem et al., 2001). Atkinson assumed the existence of a spatial relationship between and inside pixels to determine the location of different classes in the sub-pixel scale with respect to the output of the initial image fuzzing process (Atkinson, 1997).

Several other factors such as the type of complication, the genus of the earth, the time of imaging plays an important role in the accuracy of extraction of information from satellite imagery. In satellite images, in majority of pixels there is a mixture of coatings and complications, and this affect the subject for the image analysis. Fisher believes that in

remote sensing images, pixels can be broken into smaller pixels, provided that the original pixel values are given to the sub-pixels (Fisher, 1997).

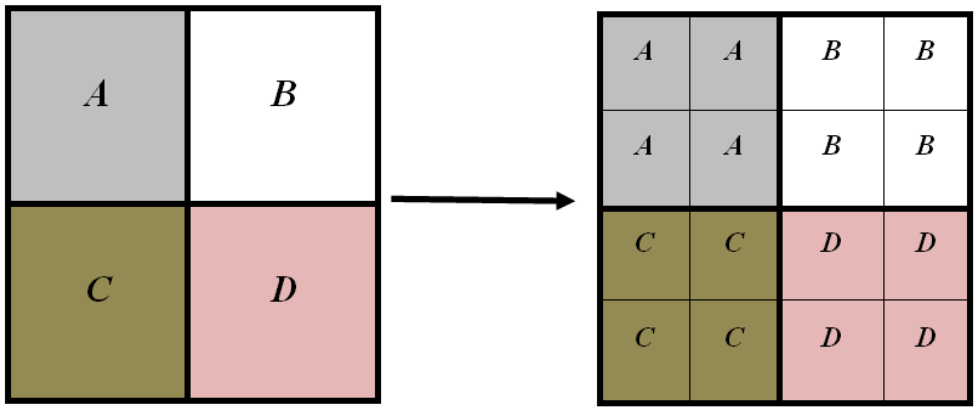


**Figure 1.** How to break the pixels and set it to the Fisher method

Super-resolution land cover mapping (SRM) (or sub-pixel mapping) is a technique applied to generate land cover maps with finer spatial resolution than the input data (Atkinson, 1997, 2009). This technique has been used for land cover mapping (Tatem et al., 2003; Thornton et al., 2006), waterline mapping (Foody et al., 2005), floodplain inundation mapping (Huang et al., 2014), urban building mapping (Ling et al., 2012b), urban tree mapping (Ardila et al., 2011), and the landscape pattern indices accuracy improvement (Li et al., 2011).

SRM can be categorized into two groups, according to the input data. One group is applied directly on remotely sensed images, including Markov random field based SRM (Li et al., 2012b), SRM with constrained linear spectral un-mixing model (Ling et al., 2012a), and FCM-based SRM (Li et al., 2012a). The other group is applied to land cover fraction images, which are the output of spectral un-mixing or soft classification applied to remotely sensed images. This group of SRM methods involve pixel-swapping model (Su et al., 2012b; Tong et al., 2013), indicator geostatistics based model (Boucher and Kyriakidis, 2006), multiple-point simulation based model (Ge, 2013), linear optimization (Verhoeye and De Wulf, 2002), spatial attraction (Ling et al., 2013b), genetic algorithm (Mertens et al., 2003), interpolation based model (Ling et al., 2013a; Wang et al., 2014b), Hopfield neural network (Muad, 2011; Su et al., 2012a), back propagation neural network (Wu et al., 2011), artificial immune systems based model (Zhong and Zhang, 2013) and multi-scale information based model (Ling et al., 2014).

Another super-resolution HNN-based algorithm was used based on the use of fuzzy output to restrict the energy function (Tatem et al., 2001; Tatem et al., 2001b), in this algorithm, a more precise method has been used for this task, in which the values of the sub-pixel are different with the original pixel values, and this property has the following advantages:

a) Improve the categorization and location in sub-pixel scale

b) Calculation of different land covers with a much higher accuracy
c) Diagnosis of urban objects with higher precision

This algorithm achieved significant success with semi-natural effects, but there is still problem of uncertainty due to the varied complexity in the final reflectance recorded by the sensors.

In another article, the shift and partial change in the position of the effects in the sub-pixel range is used, so that satellite images are collected for a specific location for several days, but the images are not exactly the same due to minor changes in the orbital coordinates of the satellite. You can identify the details of the effects by applying a few images (Ling et al., 2010). In this method, the input parameters of the neural network model were applied with artificial images and the model was implemented for the state of an image, four images, eight images and twelve images, and the improvement of the map accuracy proportional to the increase of the number of images used in the model have been confirmed (Ling et al., 2010).

Xiaodong and his cooperators present a spatial–temporal Hopfield neural network (STHNN) based SRM, by employing both a current coarse-resolution image and a previous fine-resolution land cover map as input (Xiaodong et al., 2014).

Since it is necessary to study the accuracy of the super-resolution algorithm for various complications in terms of tissue, size and imaging sensors, the results should be applied to improve the efficiency of the method. In this study, Super-Resolution algorithm (Hopfield Neural Network) has been using on images of the MODIS and OLI sensors, to examine the results of different effects and prioritize them, which are considered as aspects of innovation in this study.

Despite the wide variety of image complications, it seems that if the super-resolution algorithm is applied to a part of the image (separating the desired frame of the image) constant results are obtained in the accuracy of the extraction of the land covers. Also, the accuracy of the super-resolution algorithm seems to gives different outcomes with different land covers tissues so that they are detected and revealed more uniformly and homogeneously with the borders of the homogeneous tissues. Another hypothesis is that depending on the geometric shape of the land cover, results of the super-resolution algorithm will change in such a way that when the circularity parameter is higher, results in better face detection. The other hypothesis by using super-resolution algorithm can locate and determine the objects with point effects on sub-pixel scale.
The general objective of this research is to investigate the Hopfield neural network and achieve a meaningful result in detecting various land covers, by considering the type of land cover and sensory in case of sustainability, the optimal complication categorized for the corresponding sensor is based on the method described above. It is obvious that each of the applied fields of this algorithm can be considered as a specific goal and will result in better extraction of sub-pixel scale land cover and determine the exact boundary achieved for various land covers, which is one of the main objective of remote sensing.

## 2. Research Methodology

### 2.1. Location and characteristics of the studied land covers and input maps for the algorithm

Present research is an applied research using Hopfield neural network algorithm on MODIS images and controlling the results with Landsat images. For this purpose, after reviewing the images, the MODIS images include the appropriate spatial land cover classes with acceptable dimensions for use in the selected super-resolution algorithm and raw images were downloaded from the website http://ladsweb.nascom.nasa.gov/data/search.html, corresponding to MODIS images and location of the target land covers of the algorithm, relative Landsat images were downloaded with the shooting time approximately same as MODIS images, from the website http://earthexplorer.usgs.gov. After the initial study, four images of the MODIS sensor included an Aqua satellite image of March 18, 2016, with a resolution of 250 m from Lavan Island in the Persian Gulf, an Aqua satellite image of July 15, 2016, with a resolution of 250 m Rice fields located in Fars province, a Terra satellite image of April 3, 2016, with a resolution of 250 meters from Sargamish Lake in Turkmenistan and a Terra satellite image of June 17, 2015, with a spatial resolution of 250 m from the vegetation area located in South of the Alborz mountain, and the same number of OLI Landsat8 images are provided for the target areas, coordinate system of images was set using ENVI 4.8 software and geometric correction parameters, and systematic errors, radiometric errors, etc., were corrected and deleted as much as possible, then the images were classified fuzzy and was used as the input data of the algorithm.

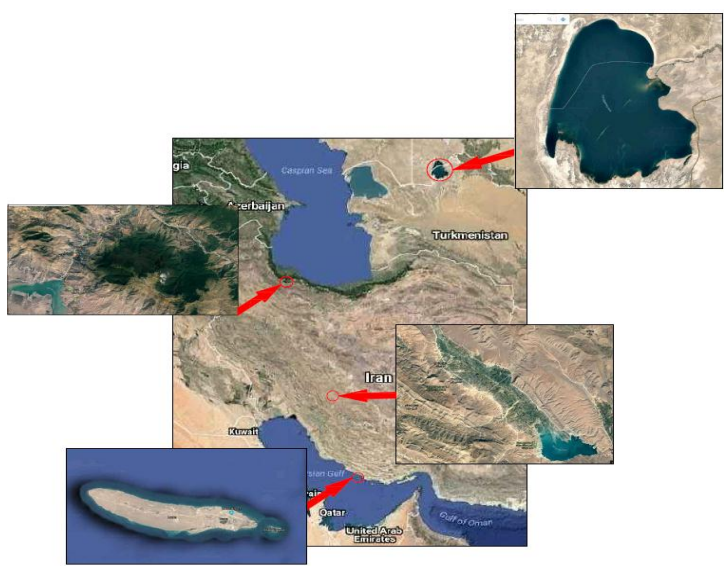


**Figure 2.** Location of the land cover

## 2.2. Designing the Neural Network (zoom factor)

In order to allow the entry into the sub-pixel scale, each pixel of the image is converted into z * z network of neurons (actuators) and through these neurons which are at the sub-pixel scale are responsible for determining the location of the effects. According to the pixel values the access to the sub-pixel range has been provided, thereby to improve the classification and the possibility to determine the exact location of the land cover on a smaller scale than the pixel dimensions of the image which can be verified.

The value of z depends on the conditions of the studied case and can be determined optimally according to the results of the algorithm so that; if increase of z does not have a positive effect on the improvement of the results of the algorithm, as increase in z leads to the sharp reduced convergence rate of the algorithm, so as to optimally design the size of neuron network.

In Figure 3, each neuron matrix indicates a land cover class and each neuron (i, j) represents a sub-pixel in the position (i, j).

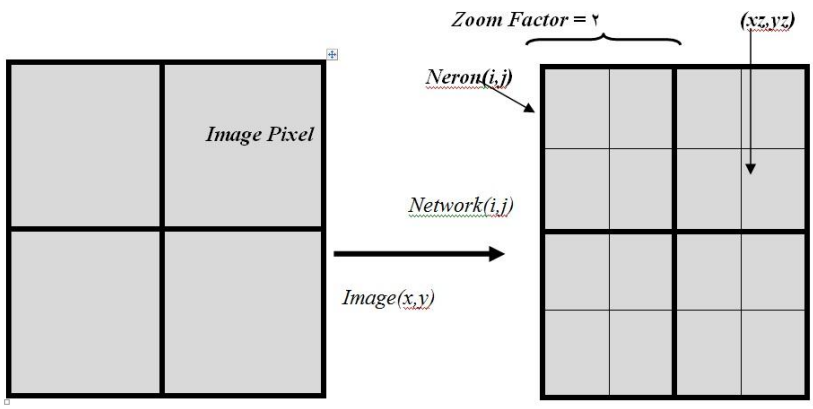


**Figure 3.** Converting the image to the neuron network

## 2.3. Primary initialization method to neuron network

In this research, the primary initialization is made intelligently according to proportion of the land cover class in pixels. Based on the principle of spatial correlation of natural phenomena, the neurons close to the center of gravity of the adjacent pixels belonging to the particular class get higher values. This initialization method is used to double the speed of network implementation in the periods of repetition and high zoom factors and the probable bias in the path of the algorithm is acceptable.

## 2.4. How to implement the algorithm?

In the Hopfield Neural Network (HNN) method, the spatial distribution of the class of land cover at pixel level is defined as formulas and is achieved by minimizing the defined function to the optimal possible state. In this method, the neurons are known by their position, such that the neuron (i, j) in row i and column j has the input value Uij and the output value Vij.

In the neural network method, first, a converted fuzzy image is transformed into a grading space, each neuron is initialized with Unit then the E function is the main equation of the HNN neural network algorithm, including the target functions and the function of the constraint (Limit) is defined as follows:

$$\text{Energy} = \text{Goal} + \text{Constraint} \quad (1)$$

$$E = -\sum i \sum j \, (k1G1ij + k2G2ij + k3Pij) \quad (2)$$

$$dEij / dvij = k1(dG1ij / dvij) + k2(dG2ij / dvij) + k3(dPij / dvij) \quad (3)$$

$$\frac{d\,G1ij}{d\,Vij} = \frac{1}{2}(1 + \tanh(\frac{1}{8}\sum_{\substack{k=i-1 \\ k\neq i}}^{i+1}\sum_{\substack{l=j-1 \\ l\neq j}}^{j+1}(v_{kl} - 0.5))l)\times(vij - 1) \quad (4)$$

$$\frac{d\,G2ij}{d\,Vij} = \frac{1}{2}(1 + (-\tanh(\frac{1}{8}\sum_{\substack{k=i-1 \\ k\neq i}}^{i+1}\sum_{\substack{l=j-1 \\ l\neq j}}^{j+1}(v_{kl}))l)) \times vij \quad (5)$$

k1, k2, k3: constant coefficient of weight of various parameters of the energy function G1ij, G2ij: The values of the output of the neuron (i, j) for the two target functions Pij: The values of the output of the neuron (i, j) for the constraint function.

The energy function E must be minimized, which means that the resultant target functions (G1 & G2) and the constraint function P are the lowest values. This equation is repeated until the difference in the output values of the neurons for two consecutive periods is less than ≦ (Epsilon).

$$\sum ij \, (Uij(t+dt) - Uij(t)) < = ™ \quad (6)$$

In this research, an algorithm function consisting of target functions, increasing and decreasing the values of neurons, and the function of limiting the membership of neurons, is based on determining the location of a particular land cover class in the sub-pixel scale by optimizing the output values Neurons are related to the natural relationships that points near each other are often more similar in nature. The degree of dissimilarity relates to the environment and the type of data harvest. These impressions can be the same pixels of satellite images, and the discovery of the relationship between pixels is used as the assumption of spatial relationships. In this study, with initialization in the range of [0.3

0.7](intelligence), so that neurons close to the center of gravity of the adjacent pixels have higher values, and finally, after executing the algorithm, we will reach a dipole map representing The location of the class is a special land cover in the sub-pixel scale.

The purpose of this algorithm is to examine the similarity of a neuron's output with respect to adjacent neurons, and if the amount of neurons (i, j) is similar to the average of 8 neurons adjacent, low energy is obtained (the energy function is minimal) And if the output of the central neuron differs from the neighbors, an undesirable condition is obtained based on the definition of spatial relationships (the points are closer to each other are more similar) and are generated a large energy for function. Therefore, for the purpose of producing a dipole map, definition of one function is inadequate, and therefore two objective functions are defined, one for increasing the amount of output of the neuron to one and the other for reducing the output value of the neuron to zero And each one depends on the average output of the 8 Neuron in neighboring.

- The first function (G1) to increase the output of the center neuron to one (vij to 1)
- The second function (G2) to reduce the output of the center neuron to zero (Vij to 0)
- Constraint function

According HNN algorithm, the objective functions will result in the assignment of zero and one outputs for each pixel, so a method to limit the effect of these functions (target functions) is required to apply the function for the areas of the image that is required. If a pixel, X percent belongs to a class, after performing the HNN algorithm and breaking the pixel to the sub-pixels, the total pixels that eventually belong to that class should provide the same percent, and the function Pij applies this limitation.

## 2.5. Practical methods to improve the efficiency of the algorithm

- Average times for each repeat period
- Define algorithm coefficients
- Zoom Factor Parameter
- Repeat period

Since the land covers differ in nature, such as roads, houses, lakes, forests, agricultural land, etc., these various effects are classified by definition of compactness and circularity parameters. In this study, the effects of the form of land covers on the final results were also examined.

| | | |
|---|---|---|
| r=a/(π*Max^2) | Circularity | (7) |
| C=(4*π*a)/(p^2) | Compactness | (8) |

a is the area of shape, p is periphery of shape and max is maximum distance from center to the edge

## 2.6. Criteria for evaluating the accuracy of the algorithm

Three main parameters were defined to evaluate the difference between the results of the algorithm implementation on different images.

### 2.6.1 Area Error Proportion

First parameter is the area error proportion which the amount of bias measured in the results of the algorithm and represents the success rate of the algorithm and is calculated from the following equation based on the output values of the neurons.

$$AEP = \frac{\sum_{q=1}^{n} (y_q - a_q)}{\sum_{q=1}^{n} a_q} \quad (9)$$

y is the degree of belonging to a particular class derived from Landsat's classified image
a is the degree of belonging to a particular class derived from the output of the algorithm
n is the number of neurons used in the algorithm

### 2.6.2 Root mean square error

The second parameter is the root mean square error, which in most of the statistical research is an appropriate criterion for accuracy checking. In this study, the accuracy of the estimation for the output values of the neurons has been used. The least squares error value is calculated by using equation 10:

$$RMSE = \sqrt{\frac{\sum_{q=1}^{n} (y_q - a_q)^2}{n}} \quad (10)$$

### 2.6.3 Correlation coefficient

The third parameter is the correlation coefficient, which provides an alternative metering to determine the dependence between the results of the algorithm and the initial images, and provides statistical information about the variance and spatial distribution in the sub-pixel range; the correlation coefficient value is computable through equation 11.

$$r = \frac{C_{y.a}}{S_y . S_a} \quad , \quad C_{y.a} = \frac{\sum_{q=1}^{n} ((\bar{y}_q - y_q).(\hat{a}_q - a_q))}{n-1} \quad (11)$$

Cy.a is covariance between y and a
Sa and Sy are standard deviation for a and y

## 3. Results and Discussion

As shown in Fig. 4, the final bipolar maps include the estimated position of the land covers in sub-pixel scale obtained after implementing the algorithm.

*a۳* *a۲* *a۱*

a1: Categorized Image OLI a2: Categorized Image MODIS a3: HNN dipole map with zoom factor 12, iteration 1000, and duration of the algorithm 30 minutes

*b۳* *b۲* *b۱*

b1: Categorized Image OLI b2: Categorized Image MODIS b3: HNN dipole map with zoom factor 12, iteration 500, and duration of algorithm execution 35 minutes

*c۳* *c۲* *c۱*

c1: Categorized Image OLI c2: Categorized Image MODIS c3: HNN dipole map with zoom factor 12, iteration 400 and duration of algorithm execution 17 min

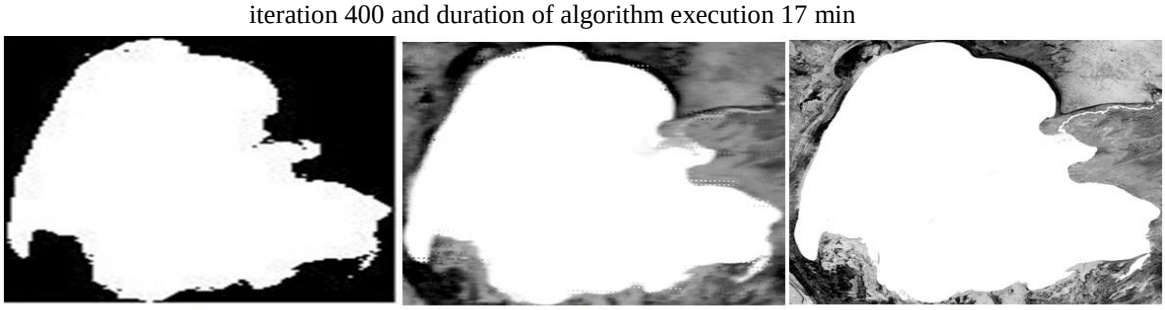

*d۳* *d۲* *d۱*

d1: Categorized Image OLI d2: Categorized Image MODIS d3: HNN dipole map with zoom factor 8, iteration 500 and duration of algorithm 125 min

**Figure 4.** Bipolar maps (a, b, c, d) obtained from the HNN algorithm with optimal zoom factor

As can be seen in the Figure 4, in case of all land covers of the study area, by increasing the magnitude of the zoom factor, the quality and accuracy of the position of land cover in the sub-pixel scale improves.

## 3.1 Process of changing the parameters of the algorithm evaluation

In Figure 5, the associated graph with the trend of changes in the parameters of the estimation of the accuracy of the algorithm (correlation coefficient, area error proportion and root mean square error) is related to land class and the use of optimized zoom factor.

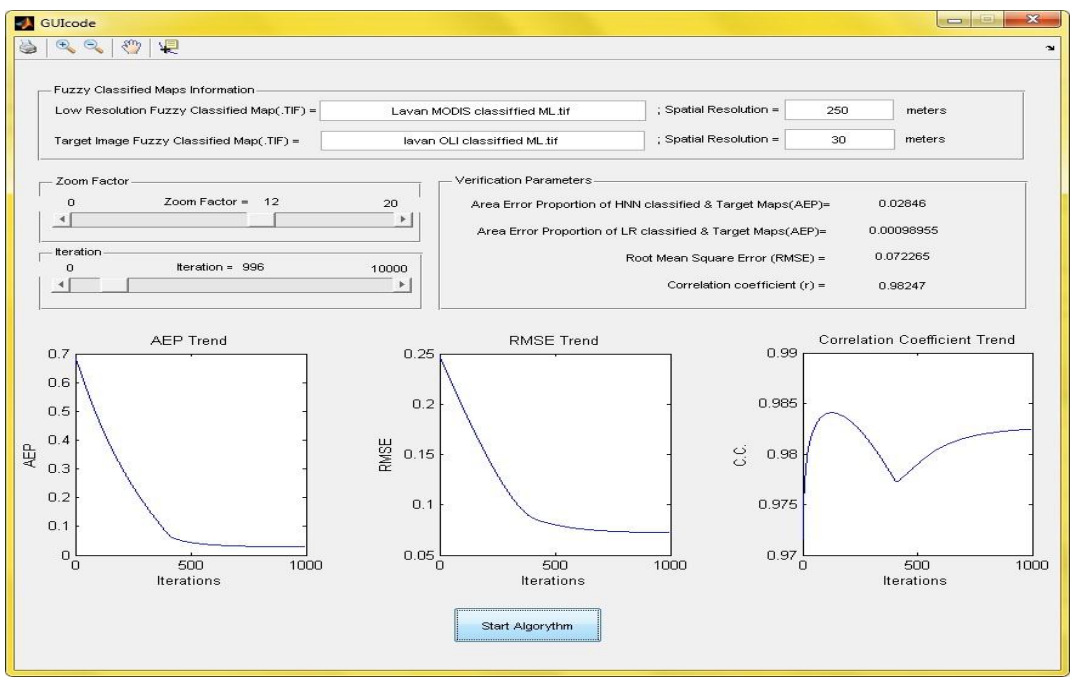


**Figure 5.** Chart of changes in the parameters of assessment of the accuracy of algorithm for land class (Lavan Island) in Optimal Factor Zoom

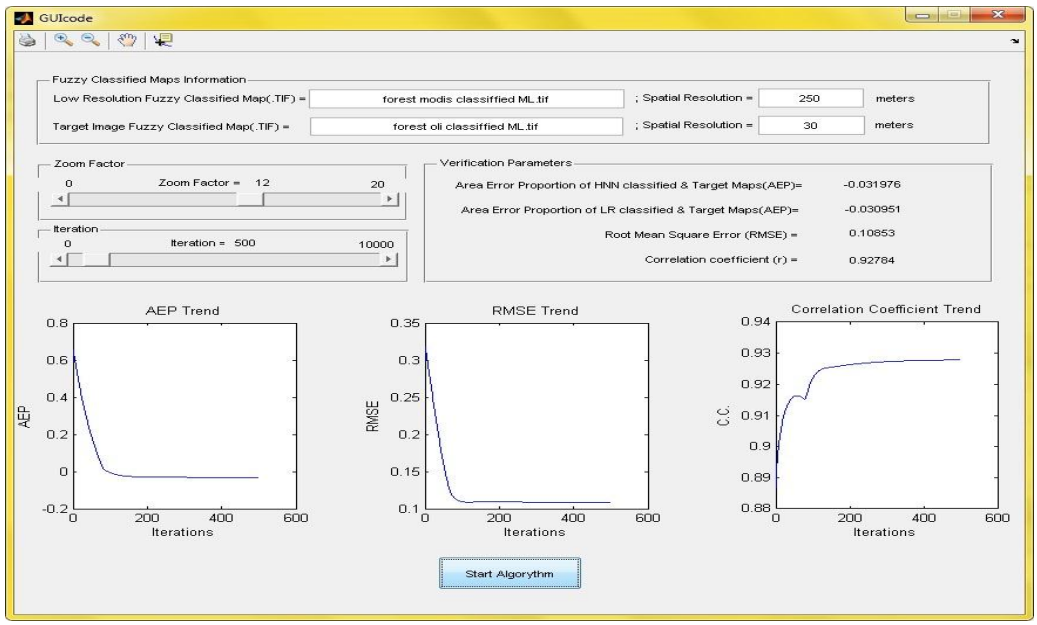


**Figure 6.** Chart of changes in the parameters of assessment of the accuracy of algorithm for vegetation class (forest) in Optimal Factor Zoom

Comparing Figures 5 and 6 the values of the relevant evaluation parameters is significant; the numerical value of the evaluation parameters shows high accuracy in detecting land class compared to the vegetation class.

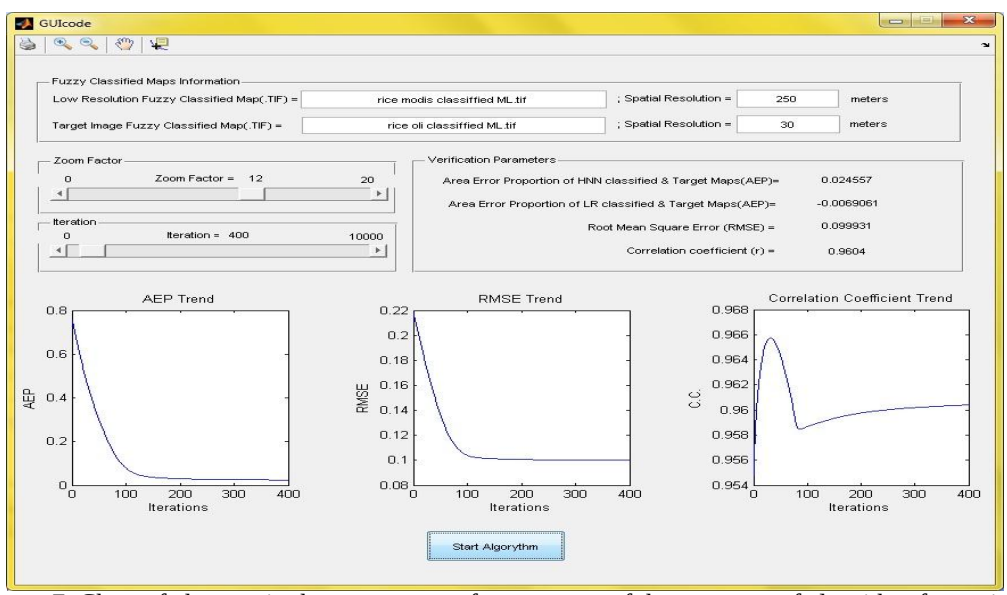


**Figure 7.** Chart of changes in the parameters of assessment of the accuracy of algorithm for agriculture class (rice) in Optimal Factor Zoom

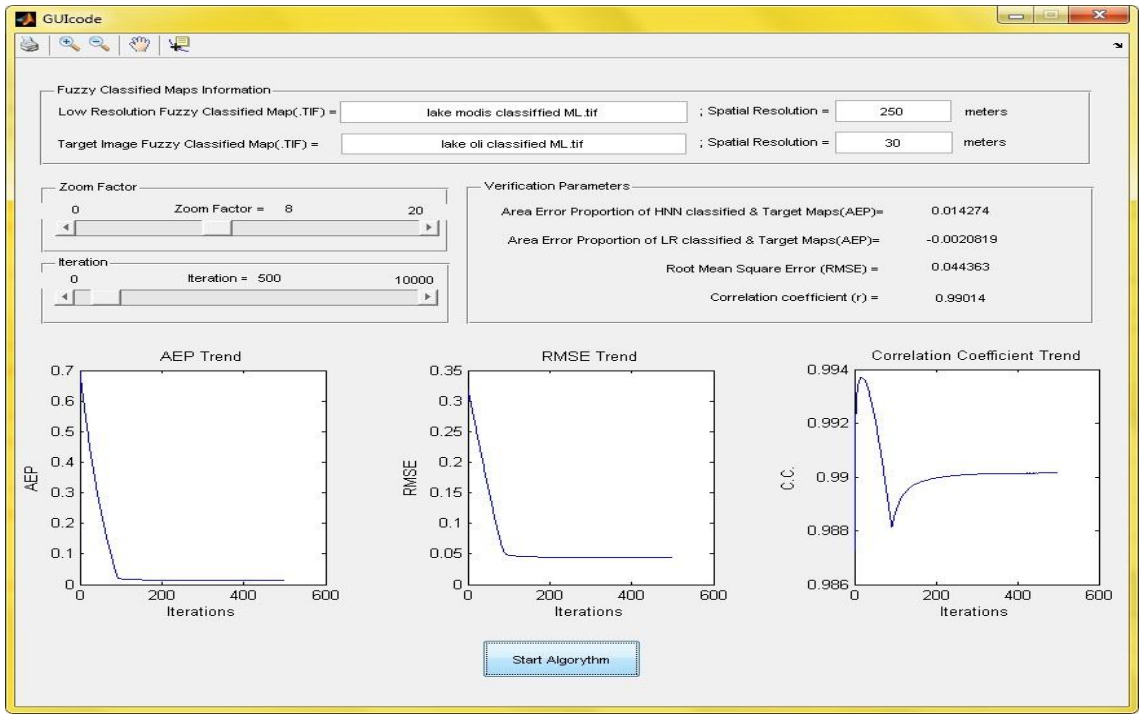


**Figure 8.** Chart of changes in the parameters of assessment of the accuracy of algorithm for water class (lake) in Optimal Factor Zoom

Comparing Figures 5, 6, 7 and 8, it is clear that the evaluation values of the relevant assessment parameters, the accuracy detection of water is higher than vegetation, land, and agriculture; accuracy detection of land class is higher relative to the land degradation under cultivation and vegetation cover; and the accuracy detection of the agriculture class is higher than the vegetation cover.

Figures 5, 6, 7, and 8 show that for zoom factor 12, the convergence process is performed rapidly and, while obtaining favorable results for the root mean square error and the area error proportion, has been done to achieve high correlation coefficient with acceptable process of change. It should be noted that, the reason for part of the high correlation coefficient is the possibility for precise classification of the input images, partly due to the wide range of land cover studied and, of course, high efficiency of the algorithm.

Also, the results show that, firstly, increasing the zoom factor while reducing the area error proportion rate, leads to a decrease in the resulting bias, which represents the success of the algorithm. Secondly, increasing zoom factor leads to a decrease in the root mean square error rate, which is a suitable criterion for measuring the accuracy of the results. Thirdly, increasing the magnification of the zoom factor increases the correlation coefficient, which indicates that there is correlation between the initial image and the outcomes.

## 3.2 Reviewing the process of improving the area of exposure

**Table 1.** Process of improving the apparent area for land class (Lavan Island)

| No | Sensor | Zoom factor | No of apparent pixels | Pixel dimension | Area ($km^2$) |
|---|---|---|---|---|---|
| 1 | OLI | ---- | 82018 | 30*30 meter | 73.816 |
| 2 | MODIS | 1 | 1140 | 250*250 meter | 71.25 |
| 3 | MODIS | 4 | 18808 | 62.5*62.5 meter | 73.46 |
| 4 | MODIS | 8 | 75773 | 31.25*31.25 meter | 73.75 |

As shown in Table 1, the apparent area of land class was improved from 71.25 to 73.75 $km^2$ and its accordance with the reference area (OLI image) indicates a high accuracy of 0.999.

**Table 2.** Process of improving the apparent area for vegetation class (forest)

| No | Sensor | Zoom factor | No of apparent pixels | Pixel dimension | Area ($km^2$) |
|---|---|---|---|---|---|
| 1 | OLI | ---- | 18559 | 30*30 meter | 162.503 |
| 2 | MODIS | 1 | 2257 | 250*250 meter | 141.063 |
| 3 | MODIS | 4 | 39447 | 62.5*62.5 meter | 158.090 |
| 4 | MODIS | 8 | 159753 | 31.25*31.25 meter | 161.327 |

As shown in Table 2, the exposed area of vegetation cover from 141.06 $km^2$ to 161.33 $km^2$ was improved and its accordance with the reference area indicates a high accuracy of 0.992.

**Table 3.** Process of improving the apparent area for agriculture class (rice)

| No | Sensor | Zoom factor | No of apparent pixels | Pixel dimension | Area ($km^2$) |
|---|---|---|---|---|---|
| 1 | OLI | ---- | 88524 | 30*30 meter | 79.672 |
| 2 | MODIS | 1 | 963 | 250*250 meter | 60.188 |
| 3 | MODIS | 4 | 18894 | 62.5*62.5 meter | 73.800 |
| 4 | MODIS | 8 | 77335 | 31.25*31.25 meter | 75.522 |

As seen in Table 3, the apparent area under cultivation improved from 60.19 $km^2$ to 75.52$km^2$, and its accordance with the reference area indicates a high accuracy of 0.948.

**Table 4.** Process of improving the apparent area for water class (lake)

| No | Sensor | Zoom factor | No of apparent pixels | Pixel dimension | Area ($km^2$) |
|---|---|---|---|---|---|
| 1 | OLI | ---- | 4517211 | 30*30 meter | 4065.49 |
| 2 | MODIS | 1 | 63157 | 250*250 meter | 3447.31 |
| 3 | MODIS | 4 | 1023821 | 62.5*62.5 meter | 3999.30 |
| 4 | MODIS | 8 | 4107981 | 31.25*31.25 meter | 4011.70 |

As shown in Table 4, the apparent surface area of water has been improved from 3947.31 $km^2$ to 4011.70 $km^2$, and its accordance with the reference area indicates a high accuracy of 0.987.

## 3.3 Accuracy check of the algorithm, depending on the shape of land cover

The specification of the land covers including area, compactness coefficient and coefficient of circularity, which is extracted using OLI images, is presented in Table 5.

**Table 5.** Characteristics of the shape of the land cover

| **No** | Location | Periphery (km) | Area $(km^2)$ | Max distance from center to edge $(km)$ | Compactness | Circularity |
|---|---|---|---|---|---|---|
| 1 | Lavan Island | 52.030 | 73.816 | 12.076 | 0.343 | 0.161 |
| 2 | Forest | 52.160 | 162.503 | 9.760 | 0.751 | 0.543 |
| 3 | Lake | 260.600 | 4,065.490 | 45.750 | 0.752 | 0.618 |
| 4 | Rice Farm | 45.600 | 79.672 | 11.500 | 0.481 | 0.192 |

Compactness and circularity parameters are extracted using OLI images. As shown in chart 1, fitted linear regression to the data confirms that, with increasing circularity and compactness, the root mean square error decreases. But, because of the great impact of the type of land covers, its texture and the accuracy of the input images classification of the algorithm in the final results, then the changes are not tangible and definitive comments in this regard are not possible.

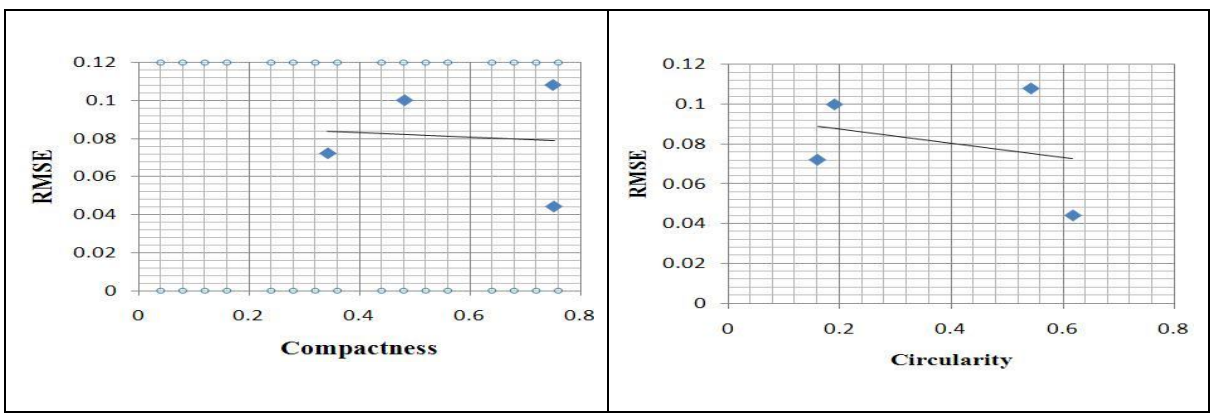


**Chart 1.** Process of changing the root mean square error values in different circularity and compactness

3.4 Review the changes in algorithm evaluation parameters regardless to land cover type

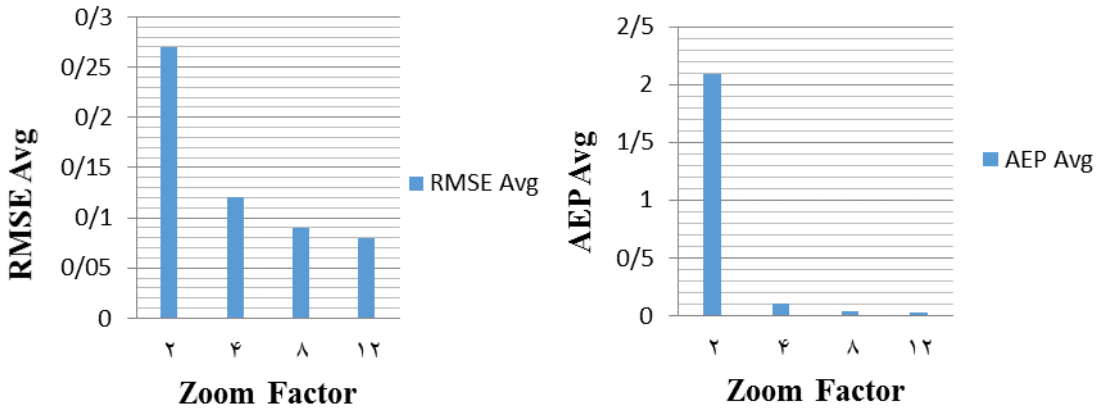


**Chart 2.** Process of changing the average area error proportion and root mean square error on different zoom factors

Chart 2 illustrates the fact that by increasing the magnitude of the zoom factor, there has been a nonlinear reduction of both parameters, average values of the root mean square error and the average values of the area error proportion level for the various classes. The obvious points in this diagram are, first, the high error in the zoom factor 2, and second is the downward decrease of the average values of the calculated errors. In the review of chart 3, it is obvious that by increasing the zoom factor magnitude, there will be an increase in the mean correlation coefficient for various land covers, a clear indication in this chart is the high correlation between the OLI high resolution classified images and the algorithm results (classification of images with low resolution of MODIS in (z = 12). Also, as can be seen, there is downward increase of correlation coefficient.

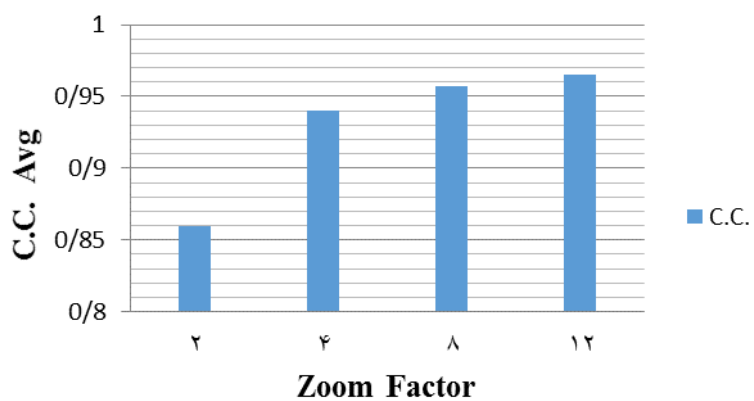


**Chart 3.** Trend of correlation Coefficient for different zoom factors

## 3.5 Performance review of the algorithm based on all parameters

**Table 6.** Characteristics of the classes and results of the algorithm

| Agriculture class | Vegetation class | Land class | Water class |
|---|---|---|---|
| 0.481 :compactness | 0.751 :compactness | 0.343 :compactness | 0.752 :compactness |
| 0.192 :circularity | 0.543 :circularity | 0.161 :circularity | 0.618 :circularity |
| 79.672 :ref. area | 162.503 :ref. area | 73.816 :ref. area | $km^2$ 4065.49 :ref. area |
| 75.52 :est. area | 161.327 :est. area | ۷۳،۷۵ :est. area | 4011.70 :est. area |
| 0.948 :Area accuracy | 0.992 :Area accuracy | 0.999 :Area accuracy | 0.987 :Area accuracy |
| 25.47 % :Improved area% | 14.3 % :Improved area% | 3.5 % :Improved area% | 1.63 % :Improved area% |
| 0.0246 : AEP | 0.032 : AEP | 0.0285 : AEP | 0.0143 : AEP |
| 0.1 : RMSE | 0.108 : RMSE | 0.0722 : RMSE | 0.0443 : RMSE |
| 0.96 :correlation Coefficient | 0.928 :correlation Coefficient | 0.982 :correlation Coefficient | 0.99 :correlation Coefficient |

By evaluation the data in Table 6 which presents the final results of the algorithm:
• Regarding the AEP parameter that represents the correctness of the algorithm, the best results for the water, agriculture, land and, the vegetation class were recorded.

• Regarding the correlation coefficient parameter, which indicates the precision of spatial distribution of the sub-pixel scale, the best results for water, land, agriculture and vegetation class were recorded.

• Regarding the accuracy parameter of the area calculation, which indicates the proximity of the detected pixels to the OLI image, the best results for land, vegetation, water and cultivated land class were recorded.

• Regarding the parameter of the percentage improvement in area that indicates the effectiveness of the algorithm for a specific class, the best results for the class of cultivated land, vegetation, land and water class were recorded.

• Regarding the RMSE parameter, which best describes the accuracy of the algorithm, the best results for the water, land, cultivated land, and, vegetation class were recorded.

Discussion

The high accuracy of the results presented in Table 6 illustrates the potential of Hopfield's Neural Network algorithm detecting accurately the location of various land cover classes on the sub-pixel scale. The land cover classes that were inspected in this study, the homogeneity and uniformity of the water class led to the high efficiency of the neural network algorithm for this class, and vice versa for vegetation cover class, due to its dispersion and irregularity in the sub-pixel scale, despite the acceptability of efficiency of the algorithm, results with lower accuracy were achieved.

According to Tables 1, 2, 3, and 4, the comparison of OLI-classified images and output maps of Hopfield's super-resolution algorithm proves the ability and efficiency of the algorithm, and the values of revealed surfaces for every land cover have a meaningful proximity to the extracted surfaces from high resolution images. This indicates the high power of the algorithm in detecting and determining the shape of the classes. Another trait

of the algorithm is the detection of the corners of the land cover classes more accurately (closer to reality) and non-abnormal fractures.

In general, in higher zoom factors, due to the access of goals function to smaller areas in the sub-pixel scale, better performance of the algorithm is achievable. With regard to the problem of detecting the corners of the classes, the initial information of the land cover shape can be used as a potential to improve the accuracy of the final maps.

As expected, in the case of vegetation and cultivated land cover, in comparison to the water and land classes, the algorithm for cover classes with complicated, heterogeneous and irregular shapes resulted with less precision. In most of the initial research, artificial images have been used as inputs to investigate the efficiency of the super-resolution algorithm using Hopfield's neural network. In another study in which asphalt and wheat fields were studied, the root mean squares error in zoom factor 5 was 0.1 for Asphalt and 0.1024 for wheat fields, and in zoom factor 7 were 0.094 and 0.088, which showed that the accuracy of the algorithm increases with increasing magnitude of the zoom factor. The values of correlation coefficient parameter, in Factor 7 for asphalt and wheat field were 0.9704 and 0.9799, respectively also the area error proportion parameter in zoom factor 7, the asphalt and wheat field were 0.001 and 0.0001. Comparing the above parameters with the results of this study, Table 6, indicates the proximity of the values and the reliability of the algorithm.

## 4. Conclusions and suggestions

### 4.1 Conclusion

The results of the five parameters evaluation, which is the accuracy of the revealed area, the percentage improvement in the exposed area, the area error proportion, the root mean square error and the correlation coefficient show that the algorithm has the best performance for the water class. The three main parameters of the area error proportion, the root mean square error and the correlation coefficient have the best results for the water class, and only two parameters related to the area do not provide significant numbers due to the high accuracy of the initialized classification map. Regarding the vegetation class, in contrast to the water class, all of the three main parameters of the evaluation of algorithm are attributed last-order to this class, which is why the vegetation in the research is in fourth place. Comparing the results of land class and cultivated land class, the land class has the second-lowest root mean square error and the second-highest correlation coefficient. In the parameter, the area error proportion is the third, and vice versa, the class of cultivated land in the two root mean square error and correlation coefficient have the third-order and second rank in the area error proportion, and these two classes in the parameters of the accuracy of the revealed area, the percentage of improvement in the area of exposure, each one has a rank, so the land class in The second place and the class of cultivated land are in the third place.

Based on the above analysis, it can be concluded that the efficiency of the HNN super-resolution algorithm on images of MODIS and OLI sensors in a sub-pixel scale presents the following ranking for revealing the classes studied in this study:

i. Water class
ii. Land class
iii. Cultivated land class
iv. Vegetation cover class

Generally, increasing the magnitude of the zoom factor from 4 to 12 leads to improve the accuracy and performance of the algorithm for all the classes and the results indicate that the use of zoom factors larger than smaller zoom factors results in more accurate detection of the corners.

Due to the low spatial resolution of the MODIS sensor, the sudden changes in the edge of the effects and the low coverage level (the effects of which are less than a pixel size) cannot be detected. Therefore, this algorithm is applicable to cases such as kilometers forest coverings, sea and lakes, large agricultural land, the extent of fire zones, flood districts, desertification affected areas, the identification of the fire center, military applications in the field of identifying that they create anomaly in any way in the images of the MODIS sensor.

### 4.2 Suggestion

Regarding the fire complication due to its high anomaly in thermal bands of MODIS sensor and the effect on adjacent pixels, it is possible to determine the edge of the feature class by means of this algorithm more precisely to the point of fire location. This brings a great deal in the direction of discovering a fire point and a faster presence to extinguish and prevent it from spreading.

It is also possible to change the structure of the HNN algorithm, such as how to initialize, how to apply coefficients for different classes depending on compactness and circularity parameters, how to change the averaging method of neurons, how to increase and decrease the values of neurons for each repeat, improved algorithm performance.

## References

Atkinson, P. M. (1997). Mapping sub-pixel boundaries from remotely sensed images. Innovations in GIS, 4, 166–180.

Atkinson, P.M.(2009). Issues of uncertainty in super-resolution mapping and their implications for the design of an inter-comparison study. International Journal of Remote Sensing, 30, 5293–5308.

Ardila, J. P., Tolpekin, V. A., Bijker, W., & Stein, A. (2011). Markov-random-field-based super-resolution mapping for identification of urban trees in VHR images. ISPRS journal of photogrammetry and remote sensing, 66(6), 762–775.

Boucher, A., & Kyriakidis, P. C. (2006). Super-resolution land cover mapping with indicator geostatistics. Remote Sensing of Environment, 104(3), 264–282.

Fisher, P. (1997). The pixel: a snare and a delusion. International Journal of Remote Sensing, 18(3), 679–685.

Foody, G. M., Muslim, A. M., & Atkinson, P. M. (2005). Super-resolution mapping of the waterline from remotely sensed data. International Journal of Remote Sensing, 26(24), 5381–5392.

Ge, Y. (2013). Sub-pixel land-cover mapping with improved fraction images upon multiple-point simulation. International Journal of Applied Earth Observation and Geoinformation, 22, 115–126.

Huang, C., Chen, Y., & Wu, J. (2014). DEM-based modification of pixel-swapping algorithm for enhancing floodplain inundation mapping. International journal of remote sensing, 35(1), 365–381.

Ling, F., Du, Y., Xiao, F., Xue, H., & Wu, S. (2010). Super-resolution land-cover mapping using multiple sub-pixel shifted remotely sensed images. International Journal of Remote Sensing, 31(19), 5023- 5040 DOI: 10.1080/01431160903252350

Li, X., Du, Y., Ling, F., Wu, S., & Feng, Q. (2011). Using a sub-pixel mapping model to improve the accuracy of landscape pattern indices. Ecological Indicators, 11(5), 1160–1170.

Lu, D., Moran, E., & Hetrick, S. (2011b). Detection of impervious surface change with multi-temporal Landsat images in an urban-rural frontier. ISPRS Journal of Photogrammetry and Remote Sensing, 66(3), 298–306.

Li, X., Ling, F., & Du, Y. (2012a). Super-resolution mapping based on the supervised fuzzy c-means approach. Remote Sensing Letters. 3(6), 501–510.

Li, X., Du, Y., & Ling, F. (2012b). Spatially adaptive smoothing parameter selection for Markov random field based sub-pixel mapping of remotely sensed images. International journal of remote sensing, 33(24), 7886–7901.

Ling, F., Du, Y., Xiao, F., & Li, X. (2012a). Subpixel land cover mapping by integrating spectral and spatial information of remotely sensed imagery. IEEE Geoscience and Remote Sensing Letters, 9(3), 408-412.

Ling, F., Li, X., Xiao, F., Fang, S., & Du, Y. (2012b). Object-based sub-pixel mapping of buildings incorporating the prior shape information from remotely sensed imagery. International Journal of Applied Earth Observation and Geoinformation, 18, 283–292.

Ling, F., Du, Y., Li, X., Li, W., Xiao, F., & Zhang, Y. (2013a). Interpolation-based super-resolution land cover mapping. Remote sensing letters, 4(7), 629–638.

Ling, F., Li, X., Du, Y., & Xiao, F. (2013b). Sub-pixel mapping of remotely sensed imagery with hybrid intra-and inter-pixel dependence. International journal of remote sensing, 34(1), 341–357.

Ling, F., Du, Y., Li, X., Zhang, Y., Xiao, F., Fang, S., Li, W. (2014). Superresolution land cover mapping with multiscale information by fusing local smoothness prior and downscaled coarse fractions. IEEE Transactions on Geoscience and Remote Sensing, 52(9), 5677-5692. http://dx.doi.org/10.1109/TGRS.2013.2291902.

Mertens, K. C., Verbeke, L. P. C., Ducheyne, E. I., & De Wulf, R. R. (2003). Using genetic algorithms in sub-pixel mapping. International Journal of Remote Sensing, 24(21), 4241–4247.

Muad, A. M. (2011). Super-resolution mapping (Doctoral dissertation, University of Nottingham).

Su, Y. F., Foody, G. M., Muad, A. M., & Cheng, K. S. (2012a). Combining Hopfield neural network and contouring methods to enhance super-resolution mapping. IEEE Journal of Selected Topics in Applied Earth Observation and Remote Sensing, 5(5), 1403–1417.

Su, Y. F., Foody, G. M., Muad, A. M., & Cheng, K. S. (2012b). Combining pixel swapping and contouring methods to enhance super-resolution mapping. IEEE Journal of Selected Topics in Applied Earth Observation and Remote Sensing, 5(5), 1428–1437.

Tatem, A. J., Lewis, H. G., Atkinson, P. M., & Nixon, M. S. (2001). Super-resolution target identification from remotely sensed images using a Hopfield neural network. IEEE Transactions on Geoscience and Remote Sensing, 39(4), 781–796.

Tatem, A. J., Lewis, H. G., Atkinson, P. M., & Nixon, M. S. (2001b). Multiple-class land-cover mapping at the sub-pixel scale using a Hopfield neural network. International Journal of Applied Earth Observation and Geoinformation, 3(2), 184–190.

Tatem, A. J., Lewis, H. G., Atkinson, P. M., & Nixon, M. S. (2003). Increasing the spatial resolution of agricultural land cover maps using a Hopfield neural network. International Journal of Geographical Information Science, 17(7), 647–672.

Thornton, M.W., Atkinson, P. M., & Holland, D. A. (2006). Sub-pixel mapping of rural land cover objects from fine spatial resolution satellite sensor imagery using super-resolution pixel-swapping. International Journal of Remote Sensing, 27(3), 473–491.

Tong, X. H., Zhang, X., Shan, J., Xie, H., & Liu, M. (2013). Attraction-repulsion model-based subpixel mapping of multi-/hyperspectral imagery. IEEE Transaction on Geoscience and Remote Sensing, 51(5), 2799–2814.

Verhoeye, J., & De Wulf, R. (2002). Land cover mapping at sub-pixel scales using linear optimization techniques. Remote Sensing of Environment, 79(1), 96–104.

Wang, Q., Shi, W., & Atkinson, P. M. (2014b). Sub-pixel mapping of remote sensing images based on radial basis function interpolation. ISPRS Journal of Photogrammetry and Remote Sensing, 92, 1–15.

Wu, K., Niu, R., Wang, Y., Zhang, L., & Du, B. (2011). Super-resolution land-cover mapping based on the selective endmember spectral mixture model in hyperspectral imagery. Optical Engineering, 50(12), 126201.

Xiaodong, L., Feng, L., Yun, D., Qi, F., & Yihang, Zh. (2014). A spatial-temporal Hopfield neural network approach for super-resolution land cover mapping with multi-temporal different resolution remotely sensed images. ISPRS Journal of Photogrammetry and Remote Sensing, 93, 76–87. http://dx.doi.org/10.1016/j.isprsjprs.2014.03.013

Zhong, Y., & Zhang, L. (2013). Sub-pixel mapping based on artificial immune systems for remote sensing imagery. Pattern Recognition, 46(11), 2902–2926.